

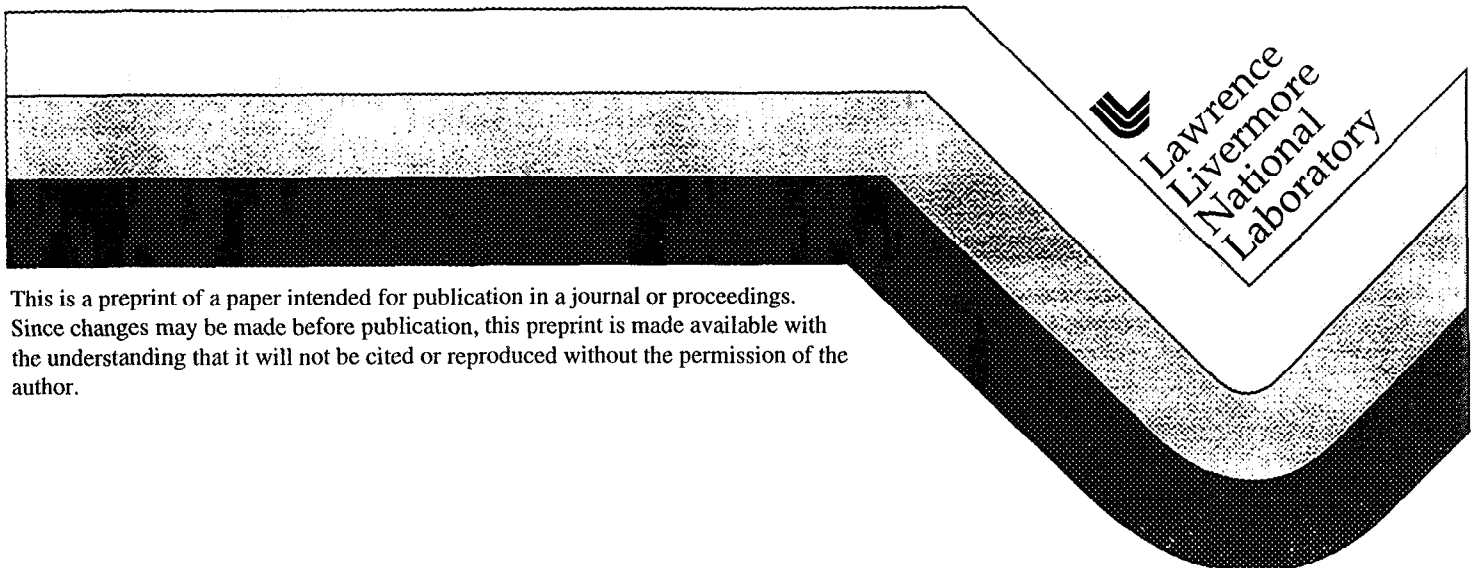
UCRL-JC-130339
PREPRINT

Shock Transformation of Deuterium from Molecular Fluid Insulator to Liquid Metal

P. M. Celliers, G. W. Collins, L. B. Da Silva, D. M. Gold, R. Cauble,
R. J. Wallace and M. E. Foord

This paper was prepared for submittal to
Nature

March 31, 1998



This is a preprint of a paper intended for publication in a journal or proceedings.
Since changes may be made before publication, this preprint is made available with
the understanding that it will not be cited or reproduced without the permission of the
author.

DISCLAIMER

This document was prepared as an account of work sponsored by an agency of the United States Government. Neither the United States Government nor the University of California nor any of their employees, makes any warranty, express or implied, or assumes any legal liability or responsibility for the accuracy, completeness, or usefulness of any information, apparatus, product, or process disclosed, or represents that its use would not infringe privately owned rights. Reference herein to any specific commercial product, process, or service by trade name, trademark, manufacturer, or otherwise, does not necessarily constitute or imply its endorsement, recommendation, or favoring by the United States Government or the University of California. The views and opinions of authors expressed herein do not necessarily state or reflect those of the United States Government or the University of California, and shall not be used for advertising or product endorsement purposes.

**Shock transformation of deuterium from molecular fluid insulator
to liquid metal**

P.M. Celliers, G.W. Collins, L. B. Da Silva, D. M. Gold,

R. Cauble, R.J. Wallace and M.E. Foord

Lawrence Livermore National Laboratory,

P.O. Box 808, Livermore, California, 94551

The transformation of hydrogen at high pressures and temperatures from an insulating molecular fluid to a monatomic metallic fluid is relevant to models of planetary and stellar interiors^{1, 2} and has important practical consequences in the application of inertial confinement fusion^{3, 4}. The search for hydrogen metallization on the cold compression curve has not yielded strong evidence for an insulator-metal transition up to pressures of 250 GPa⁵⁻⁷. At higher temperatures the first experimental demonstration of hydrogen metallization at high pressure was reported by Weir *et al.*⁸, who used a dynamic compression technique to produce band gap closure in the molecular fluid at pressure 140 GPa, molar density 0.3 mol/cm³ and temperature ~3000 K. Recent experiments using an intense laser to compress deuterium up to 200 GPa have reported high compressibility on the principal Hugoniot above 25 GPa⁹. Some equation-of-state

models of hydrogen predict this high compressibility^{10, 11} while others do not^{12, 13}. Here, we describe measurements of the optical reflectivity of the shock front which show that the high compressibility observed above 25 GPa on the Hugoniot coincides with a transformation from molecular fluid to liquid metal.

The experimental arrangement for measuring laser-driven shock waves in liquid deuterium is similar to that described previously⁹. The sample cell is sketched in Figure 1. Using one beam of the Nova laser¹⁴ we generate a high pressure shock wave in a pusher material (either Al or Be). Behind the pusher is a volume filled with the liquid deuterium sample, at density 0.17 g cm^{-3} and temperature 20 K. The shock wave transmitted through the pusher releases into the deuterium sample and generates a shock in the deuterium. Since there is a large density mismatch at the pusher-deuterium interface, the shock amplitude transmitted into the deuterium is lower than in the pusher and a reflected rarefaction propagates back through the pusher. After the shock emerges from the pusher rear surface the pusher-deuterium interface moves at constant velocity behind the shock front in the deuterium. A second beam of Nova generates an x-ray source that allows us to measure radiographically the positions of the shock front and the pusher-deuterium interface as a function of time (not shown here). From this information we determine the pressure and density in the shock compressed fluid using the Rankine-Hugoniot relations.¹⁵

We probed the reflectivity of the shock front using a 15 ns FWHM laser pulse from an injection-seeded Q-switched Nd:YAG laser, operating at 1064 nm. The pulse illuminated the sample through a sapphire window. A 150 mm focal length $f/3$ objective collected the reflected

light to form an image of the target surface in a velocity interferometer¹⁶ which was further relayed onto a streak camera slit. Details of this experimental arrangement will be presented elsewhere.¹⁷ A streak camera recorded the reflected light intensity along one spatial dimension and streaked it in time along the other dimension. The recorded signal contains a fringe pattern produced by the velocity interferometer. Doppler shifts in the light reflected from the target are manifested as fringe shifts at the output of the velocity interferometer. The fringe phase ϕ (in radians) is related to the velocity u of the reflecting surface through the velocity interferometer equation¹⁶ $\lambda\phi/4\pi\tau(1+\delta) = u$, where λ is the laser wavelength, τ is the time delay in the velocity interferometer, and $\delta = 0.017$ is a wavelength dependent correction.¹⁸ We extract ϕ from a fit of the observed fringe intensity I to a sinusoidal function: $I(x,t) = A(x,t) + B(x,t)\sin(\phi(x,t))$. With this procedure we obtain an accurate (~ 1 -2%) time- and space-resolved measurement of the shock front velocity.

Example recordings of this type of data are shown in Figure 2. For negative times on the scale in Figure 2(a) the recording shows the reflection from the stationary Al pusher surface prior to the emergence of the shock into the deuterium sample. For positive time the recording shows light reflected from the shock front. When the shock emerges from the Al interface the reflected signal drops simultaneously with a shift of the fringe pattern to a new phase. From the shift in the fringe phase we determine the shock velocity and from the reflected intensity we determine the shock front reflectivity (relative to that of the pusher surface). We extract absolute reflectivity by referencing to the reflected intensity of the motionless pusher prior to the shock breakout. We assumed reflectivities of $85\pm 10\%$ for the Al pushers¹⁹ (diamond turned

substrates) and $45 \pm 15\%$ for the Be pushers.²⁰ We have verified that the reflection observed subsequent to shock breakout indeed originates directly from the shock front. By integrating the velocity inferred from the fringe phase we reproduced the shock trajectory (position as a function of time) observed simultaneously using the x-ray radiographic measurement.¹⁷

The experiment in Figure 2(a) was designed with hydrodynamic computer simulations to produce a steady shock in the deuterium, and as such there is little observable fringe motion subsequent to the shock breakout. This particular measurement represents one datum of shock reflectivity as a function of shock speed. Shown in Figure 3 are results obtained a series of such measurements for several drive conditions and pusher types with shock speeds ranging from 19 $\mu\text{m/ns}$ to 55 $\mu\text{m/ns}$ and corresponding to Hugoniot pressures ranging from 55 GPa to approximately 400 GPa. The higher amplitude results were obtained using Be pushers.

To obtain a wider range of observed velocities and to examine states at lower shock amplitude we performed two additional experiments specially designed to produce a decaying shock propagating into the deuterium. We drove the Al pusher with a short (1 ns) high pressure pulse, which allowed a rarefaction to overtake the shock propagating in the Al pusher before it reached the deuterium. Figure 2(b) shows a data record obtained from one of these experiments. Clearly observable is a continuous change in the fringe phase from the velocity interferometer accompanied by a decrease in reflected light intensity as the shock front decayed. We determined the reflectivity throughout this range of velocities by comparing the reflected pulse to a reference pulse recorded immediately prior to the experiment, which was needed to account for temporal variation in the illumination pulse intensity. Since the shock was not steady the compressed

material behind it contained spatial density gradients along the propagation direction; however the gradient scale length ($\sim 1800 \mu\text{m}$) is much larger than the skin depth of the reflected light $\sim 0.1 \mu\text{m}$. Therefore our measurement of reflectivity of the continuously decaying shock should yield the same results as a series of measurements of steady shocks spanning the same range of velocities. At the lowest observable shock speed we found a reflectivity of approximately 3.5% at $13.4 \mu\text{m/ns}$. This reflectivity increased to an asymptotic level of approximately 60 to 65% for shock velocities greater than $20 \mu\text{m/ns}$. The corresponding Hugoniot pressures span the range from 22 – 55 GPa according to Hugoniot data.^{9, 21}

The shock front is a transition contained within a few dozen atomic spacings which is much smaller than the wavelength of the probe light and it presents a surface that has been demonstrated to be specularly smooth.²² Therefore, to a very good approximation it is a step interface and is amenable to Fresnel analysis of the reflectivity. The Fresnel formula for reflectivity at the shock front is $R = \left| \frac{\hat{n}_s - n_0}{\hat{n}_s + n_0} \right|^2$ where \hat{n}_s is the (complex) refractive index behind the shock front and $n_0 = 1.13$ is the refractive index in the undisturbed liquid. The refractive index of shock-compressed dielectrics has been found to follow the empirical Gladstone-Dale relationship, $n - 1 \propto \rho$, where ρ is the density.²² Using this scaling, and assuming the fluid remains mostly in its molecular form under shock compression the refractive index at six-fold compression would be $\hat{n}_s \sim 1.8$. The largest possible dielectric-dielectric reflectivity one could expect with this refractive index is $\sim 5\%$. Therefore, the shocked fluid must be ionized and we continue our analysis by assuming it becomes a liquid metal. Even at the extreme pressures behind the shock front measured temperatures are moderate, around 1 eV,

while the Fermi energy (assuming a metallic fluid) varies from 12 to 16 eV over the densities produced in the experiment. Since the electron fluid is Fermi-degenerate we apply the Drude conductivity model, applicable to free electron metals, which states that the complex refractive index is given by, $\hat{n}_s^2 = \epsilon_{IB} - \frac{\omega_p^2}{\omega^2}(1 + i/\omega\tau_e)^{-1}$, where ω_p is the plasma frequency, ω is the optical frequency, τ_e is the electron relaxation time, and ϵ_{IB} is a constant contribution arising from interband transitions. The plasma frequency is directly related to the degree of ionization Z , or the carrier density $n_e = Zn_i$ through the formula $\omega_p^2 = 4\pi Zn_i e^2 / m_e$, where n_i is the ion density, and e and m_e are the electronic charge and mass respectively. The most prominent feature of the Drude model is the absorption edge where the optical frequency equals the plasma frequency. This signature has been the object of several studies of hydrogen compressed in diamond anvil cells^{5, 6, 23} searching for the onset of metallization on the cold compression curve. In those studies one usually has a fixed material state (fixed ω_p , n_e or band gap as the case may be), and varies ω to observe the Drude edge. In our case the optical frequency ω is fixed and we examine the Drude reflectivity as a function of the material state (i.e. as n_e (or ω_p) and τ_e vary along the Hugoniot). Below the absorption edge (low n_e) the reflectivity depends on the constant ϵ_{IB} which determines the real part of the refractive index of the shocked fluid before it becomes conducting: the residual reflectivity is that of a dielectric-dielectric interface, and does not produce large reflectivities as discussed above. Above the edge ϵ_{IB} has less effect and the Fresnel reflectivity depends mainly on τ_e and n_e .

For our optical wavelength of 1064 nm the carrier density where the plasma frequency equals the optical frequency is $n_e = 10^{21} \text{ cm}^{-3}$. High reflectivities cannot be produced at carrier densities $n_e < 10^{21} \text{ cm}^{-3}$, independent of τ_e . At pressures slightly below our measurements (20 GPa on the Hugoniot) Nellis *et al.*²⁴ find a carrier concentration of 10^{15} cm^{-3} (0.0001% ionization) in shock compressed deuterium where it is still a molecular fluid; this carrier density would produce little observable reflectivity. Thus the reflectivities we observe come about through a significant change in the carrier density which must increase some 6 to 8 orders of magnitude from 10^{15} cm^{-3} to around $10^{21} - 10^{23} \text{ cm}^{-3}$ in the 20 - 55 GPa pressure range on the Hugoniot. In this pressure range the molar density varies from 0.13 - 0.24 mol cm^{-3} , and the average intermolecular spacing changes by about 25%.

From *dc* electrical conductivity measurements of hydrogen and deuterium compressed by single shocks (to 20 GPa)²⁴ and multiple reverberating shocks (to 140 GPa)⁸ Nellis *et al.* have inferred the band gap energy of the molecular fluid as a function of density. In all cases the temperatures were low ($< 4000 \text{ K}$) and the fluid was in a substantially molecular state, with a dissociation fraction less than 5%. Using a semiconductor model of the electrical conductivity, they found that the electronic band gap of the molecular fluid closed at a molar density of 0.3 mol cm^{-3} (1.2 g cm^{-3} for deuterium) and measured $\sigma_0 \sim 2000 (\Omega\text{cm})^{-1}$ at these conditions.⁸ The rising reflectivity we observe takes place at molar densities much *less* than this. At a molar density of 0.17 mol cm^{-3} corresponding to 35 GPa on the deuterium Hugoniot (reflectivity $\sim 25\%$), the molecular band gap energy according to Weir *et al.* is $\sim 9 \text{ eV}$.⁸ Clearly, promotion of charge carriers across this molecular band gap into conducting states through thermal ($kT \sim 1\text{eV}$)

and photoionization ($\hbar\omega = 1.2$ eV) processes is a mechanism that cannot produce the metallic reflectivities. The reflectivities we observed indicate carrier densities $n_e > 10^{21}$ cm⁻³, but apparently produced by a mechanism other than closure of the molecular band gap.

In the limit of strong shocks (> 200 GPa), we expect the fluid to be fully dissociated, fully ionized and converted into a dense plasma state. A model of dense plasma conductivity appropriate to these conditions is described by Lee and More²⁵ who estimate τ_e using Mott's formula²⁶ for the minimum conductivity of a metal near the metal-insulator transition. Mott's minimum conductivity is $\sigma_{\min} = 2\pi e^2/3\hbar R_0$, where \hbar is Planck's constant, and $R_0 = 2(3/4\pi n_i)^{1/3}$ is the interparticle spacing. These estimates are consistent with a physical picture in which the carrier mean free path near the metal-insulator transition is close to the interparticle spacing. For example using Mott's formula to evaluate the relaxation time with $\tau_e = m_e \sigma_{\min} / Z n_i e^2$ is equivalent to the statement $\tau_e \propto R_0 / v_f$ where v_f is the electron Fermi speed. With these prescriptions and assuming a density of 1 g cm⁻³, full dissociation and full ionization ($Z = 1$, $n_e \sim 3 \times 10^{23}$ cm⁻³), one finds $\sigma_{\min} \sim 4400$ (Ω cm)⁻¹; also $\tau_e = 5.2 \times 10^{-17}$ s and $\omega\tau_e \sim 0.09$ at the 1064 nm Nd:YAG laser wavelength. Figure 4 shows several curves of shock front reflectivity for $\omega\tau_e = 0.045, 0.09$ and 0.18 giving reflectivities ranging from 40% to 70%. Our observed 65% reflectivity is consistent with $\omega\tau_e \sim 0.18$, or a *dc* conductivity $\sigma_0 \sim 8700$ (Ω cm)⁻¹, twice the value of the Mott minimum conductivity. Theoretical calculations of the electrical conductivity of dense hydrogen plasmas²⁷ give $\sigma_0 \sim 10^5$ (Ω cm)⁻¹ corresponding to $\omega\tau_e \sim 2$; this is similar to

alkali metal conductivities. For a fully ionized plasma this conductivity would produce ~95% reflectivity, higher than we observe.

At shock pressures less than 200 GPa and indeed at at 55 GPa where the reflectivity saturates it is likely that the fluid is only partially ionized and partially dissociated. Both n_e and τ_e and must vary through the rise in reflectivity and it is evident that both play important roles in determining the observed reflectivity. However, our observations at a single wavelength cannot be used to determine both simultaneously. From Figure 4 it is evident that the observed reflectivities of 60% cannot be explained using the fixed relaxation time estimates above unless the fluid nearly fully ionized. If we allow for longer relaxation times then the high reflectivities can be produced at lower carrier densities (partial ionization). We can account for somewhat longer relaxation times as follows. The electron Fermi speed in a partially ionized fluid depends on the electronic density of states at the Fermi energy; in the free electron model the Fermi speed has a density dependence $v_f \propto n_e^{1/3}$, implying that τ_e varies with carrier density: $\tau_e \propto n_e^{-1/3}$. The interparticle spacing can also vary because of dissociation and compression; but since $R_0 \propto n_i^{-1/3}$ the total effect amounts to a factor of 1.6 at most. Figure 4 shows two curves plotted assuming $\tau_e \propto n_e^{-1/3}$, which takes these effects into account, and provides us with an estimated lower bound on the carrier density needed to produce the observed reflectivities that is also consistent with realistic relaxation times. We infer that the observed reflectivities of 60% cannot be produced unless the carrier density is between 3×10^{22} and $1.5 \times 10^{23} \text{ cm}^{-3}$, which corresponds to a range of 10-50% ionization per atom (or 20-100% per molecule). At this level of ionization the

Fermi energy remains above 3 eV, more than 3kT at 55 GPa, and therefore still consistent with our assumption of Fermi-degenerate conditions.

The metallization beginning around 22 GPa coincides with the high compressibility previously observed on the principal Hugoniot⁹, which also begins around 25 GPa. This data therefore suggests a connection between the high compressibility and the transformation of the molecular liquid into the dissociated metallic phase. Such a connection is explicitly assumed in Holmes *et al.*¹¹ in a phenomenological model that describes a continuous dissociation of the molecular fluid directly into the monatomic metallic phase. This model was generated to account for lower than expected temperatures observed in double shock compression experiments up to 90 GPa, but it also produces compressibilities on the Hugoniot consistent with experimental observations.⁹ A more elaborate equation of state calculation due to Saumon and Chabrier¹⁰ predicts a similar transformation, and similar compressibilities on the Hugoniot. Notable in the Saumon-Chabrier model is a prediction that the insulator-metal transition can occur through a first-order phase transition, called the plasma phase transition.²⁸ Both of these theoretical treatments use the “chemical picture” to determine the thermodynamic state, and are possibly inaccurate precisely through the range of conditions where dissociation and metallization take place on the Hugoniot. A more rigorous theoretical treatment based on the restricted path integral Monte Carlo method²⁹ also reports evidence for dissociation and ionization at these conditions, and more recent studies indicate that the transformation is also accompanied by high compressibility.³⁰ Further experiments at other optical probe wavelengths will provide more information on this high pressure-high temperature transformation in deuterium.

REFERENCES:

1. Smoluchowski, R. Internal Structure and Energy Emission of Jupiter. *Nature* **215**, 691-695 (1967).
2. Hubbard, W.B. Interiors of Giant Planets. *Science* **214**, 145-149 (1981).
3. Lindl, J. Development of the indirect-drive approach to inertial confinement fusion and the target physics basis for ignition and gain. *Phys. Plasmas* **2**, 3933-4024 (1995).
4. Haan, S.W., *et al.* Design and modeling of ignition targets for the National Ignition Facility. *Phys. Plasmas* **2**, 2480-2487 (1995).
5. Mao, H.K. & Hemley, R.J. Ultrahigh-pressure transitions in solid hydrogen. *Rev. Mod. Phys.* **66**, 671-692 (1994).
6. Cui, L., Chen, N.H. & Silvera, I.F. Infrared Properties of Ortho and Mixed Crystals of Solid Deuterium at Megabar Pressures and the Question of Metallization in the Hydrogens. *Phys. Rev. Lett.* **74**, 4011-4014 (1995).
7. Ashcroft, N. Dense Hydrogen: the reluctant alkali. *Phys. World* **8**, 43-47 (1995).
8. Weir, S.T., Mitchell, A.C. & Nellis, W.J. Metallization of Fluid Molecular Hydrogen at 140 GPa (1.4 Mbar). *Phys. Rev. Lett.* **76**, 1860-1863 (1996).
9. Da Silva, L.B., *et al.* Absolute Equation of State Measurements on Shocked Liquid Deuterium up to 200 GPa (2 Mbar). *Phys. Rev. Lett.* **78**, 483-486 (1997).

10. Saumon, D., Chabrier, G. & Van Horn, H.M. An equation of state for low-mass stars and giant planets. *Ap. J. Suppl.* **99**, 713-741 (1995).
11. Holmes, N.C., Ross, M. & Nellis, W.J. Temperature measurements and dissociation of shock-compressed liquid deuterium and hydrogen. *Phys. Rev. B* **52**, 15835-15845 (1995).
12. Kerley, G.I. A Theoretical Equation of State for Deuterium, Los Alamos Scientific Laboratory LA-4776 (1972).
13. Lenosky, T.J., Kress, J.D. & Collins, L.A. Molecular-dynamics modeling of the Hugoniot of shocked liquid deuterium. *Phys. Rev. B* **56**, 5164-69 (1997).
14. Campbell, E.M. Recent results from the Nova program at LLNL. *Laser Part. Beams* **9**, 209-231 (1991).
15. Zel'dovich, Y.B. & Raizer, Y.P. Physics of Shock Waves and High-Temperature Hydrodynamic Phenomena (Academic Press, New York, 1966), p. 705
16. Barker, L.M. & Hollenbach, R.E. Laser interferometer for measuring high velocities of any reflecting surface. *J. Appl. Phys.* **43**, 4669-4675 (1972).
17. Celliers, P.M., Collins, G.W., Da Silva, L.B., Gold, D.M. & Cauble, R. Accurate measurement of laser-driven shock trajectories with velocity interferometry. *Appl. Phys. Lett.*, submitted (1998).
18. Barker, L.M. & Schuler, K.W. Correction to the velocity-per-fringe relationship for the VISAR interferometer. *J. Appl. Phys.* **45**, 3692-3 (1974).

19. Smith, D.Y., Shiles, E. & Inokuti, M. The Optical Properties of Metallic Aluminum. in *Handbook of Optical Constants of Solids* (ed. Palik, E.D.) 369-406 (Academic Press, Orlando, 1985).
20. Arakawa, E.T., Callcott, T.A. & Chang, Y.-C. Beryllium (Be). in *Handbook of Optical Constants of Solids. II* (ed. Palik, E.D.) 421-433 (Academic Press, Boston, 1991).
21. Nellis, W.J., Mitchell, A.C., van Thiel, M., Devine, G.J. & Trainor, R.J. Equation-of-state data for molecular hydrogen and deuterium at shock pressures in the range 2-76 GPa (20 - 760 kbar). *J. Chem. Phys.* **79**, 1480-1486 (1983).
22. Kormer, S.B. Optical study of the characteristics of shock-compressed condensed dielectrics. *Sov. Phys. Uspekhi* **11**, 229-54 (1968).
23. Mao, H.K., Hemley, R.J. & Hanfland, M. Infrared Reflectance Measurements of the Insulator-Metal Transition in Solid Hydrogen. *Phys. Rev. Lett.* **65**, 484-487 (1990).
24. Nellis, W.J., Mitchell, A.C., McCandless, P.C., Erskine, D.J. & Weir, S.T. Electronic Energy Gap of Molecular Hydrogen from Electrical Conductivity Measurements at High Shock Pressures. *Phys. Rev. Lett.* **68**, 2937-2940 (1992).
25. Lee, Y.T. & More, R.M. An electron conductivity model for dense plasmas. *Phys. Fluids* **27**, 1273-1286 (1984).

26. Mott, N.F. Conduction in Non-crystalline systems IX. The minimum metallic conductivity. *Phil. Mag.* **26**, 1015-1026 (1972).
27. Hubbard, W.B. & Lampe, M. Thermal conduction by electrons in stellar matter. *Ap. J. Suppl.* **18**, 297-346 (1969).
28. Saumon, D. & Chabrier, G. Fluid Hydrogen at High Density: The Plasma Phase Transition. *Phys. Rev. Lett.* **62**, 2397-2400 (1989).
29. Magro, W.R., Ceperley, D.M., Pierleoni, C. & Bernu, B. Molecular Dissociation in Hot, Dense Hydrogen. *Phys. Rev. Lett.* **76**, 1240-1243 (1996).
30. Militzer, B., Magro, W. & Ceperley, D. Fermionic Path Integral Simulations of Hot, Dense Hydrogen. *Bull. APS* **43**, 609 (1998).

ACKNOWLEDGEMENT

We wish to thank A. Ng, N. Ashcroft, T. Tajima, W.J. Nellis, N.C. Holmes and M. Ross for useful discussions and B. Hammel, J. Kilkenney, L. Wiley and B. Goodwin for support of this work. This work was performed under the auspices of the U.S. D.O.E. by LLNL under contract number W-7405-ENG-48.

FIGURE CAPTIONS:

Figure 1: Cryogenic sample cell containing the liquid deuterium sample. X-ray transparent Be windows mounted on the sides allowed for transverse viewing of the shock propagation with an x-ray microscope, as described in ref. 9.

Figure 2: Light at 1064 nm wavelength reflected from a metallic liquid deuterium shock front as observed through the velocity interferometer (a) for a steady shock; and, (b) for a decaying shock. At $t = 0$ the shock was transmitted from the pusher into the liquid sample. The phase of the fringe pattern is directly proportional to the shock velocity. In (a) the reflected signal decreased to 66% of its initial value at $t = 0$ (reflectivity $\sim 56\%$) and the shock speed was $25.4 \mu\text{m/ns}$ (the phase shifted 1.2 fringes to the right). In (b) the initial shock speed was $22.9 \mu\text{m/ns}$ (initial phase shift 3.3 fringes); the fringes shift continuously to the left (deceleration) as the shock decays; reflectivity decreases simultaneously. The images do not show reflectivity directly: in (b) the illumination pulse reached its peak at $t \sim 5 \text{ ns}$, and remained above 30% of its peak power for $5 < t < 15 \text{ ns}$.

Figure 3: Reflectivity at 1064 nm of the shock front in liquid deuterium for shock speeds from 13.4 to $53 \mu\text{m/ns}$. The open symbols are single-point measurements observed at the moment of shock breakout from the pusher-deuterium interface: diamonds from experiments with Al pushers; squares, Be pushers. The solid curves were extracted from two decaying shock experiments. The dotted curve was extracted from the record shown in Figure 1 (b), and the solid curve from a similar experiment. The vertical error bars reflect our uncertainty in the reference levels, as noted in the text. The Be pusher surfaces were rougher than the Al surfaces

and more variable in quality due to surface oxide contamination, a problem which is manifested in the scatter and larger uncertainties in the high pressure points. The indicated pressures were determined from Hugoniot data⁹.

Figure 4: Drude reflectivity at 1064 nm plotted as a function of carrier density for $\epsilon_B = 1$ and different values of the relaxation time $\omega\tau_e$: 0.045 (solid); 0.09 (dashed); 0.18 (dotted); also $\epsilon_B = 2.7$ and $\omega\tau_e = 0.09$ (open circles on solid). The remaining two curves show how the reflectivity varies with carrier density assuming that the relaxation time scales as $\omega\tau_e \propto n_e^{-1/3}$: $\omega\tau_e = 0.18$ at $n_e = 3 \times 10^{23} \text{ cm}^{-3}$ (dash-dot); and, $\omega\tau_e = 0.28$ ($= 1.6 \times 0.18$, see text) at $n_e = 3 \times 10^{23} \text{ cm}^{-3}$ (open squares on solid). The top scale shows the ionization Z per atom corresponding to the carrier density on the bottom scale at a deuterium fluid density of 1 g cm^{-3} ; at this density full ionization corresponds to $n_e = 3 \times 10^{23} \text{ cm}^{-3}$.

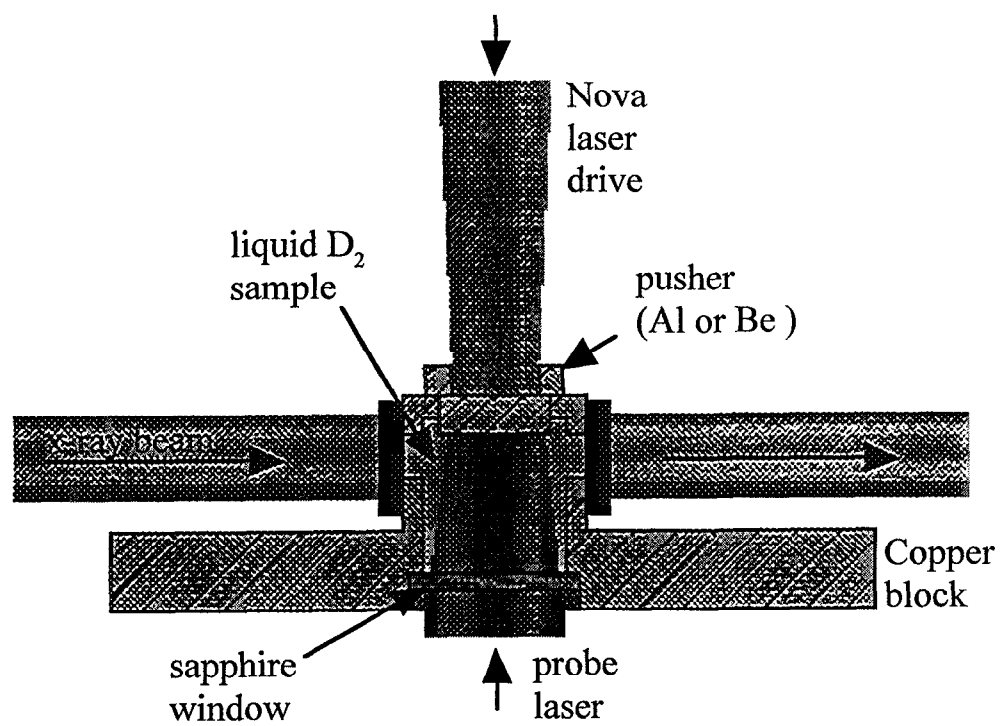


Figure 1.

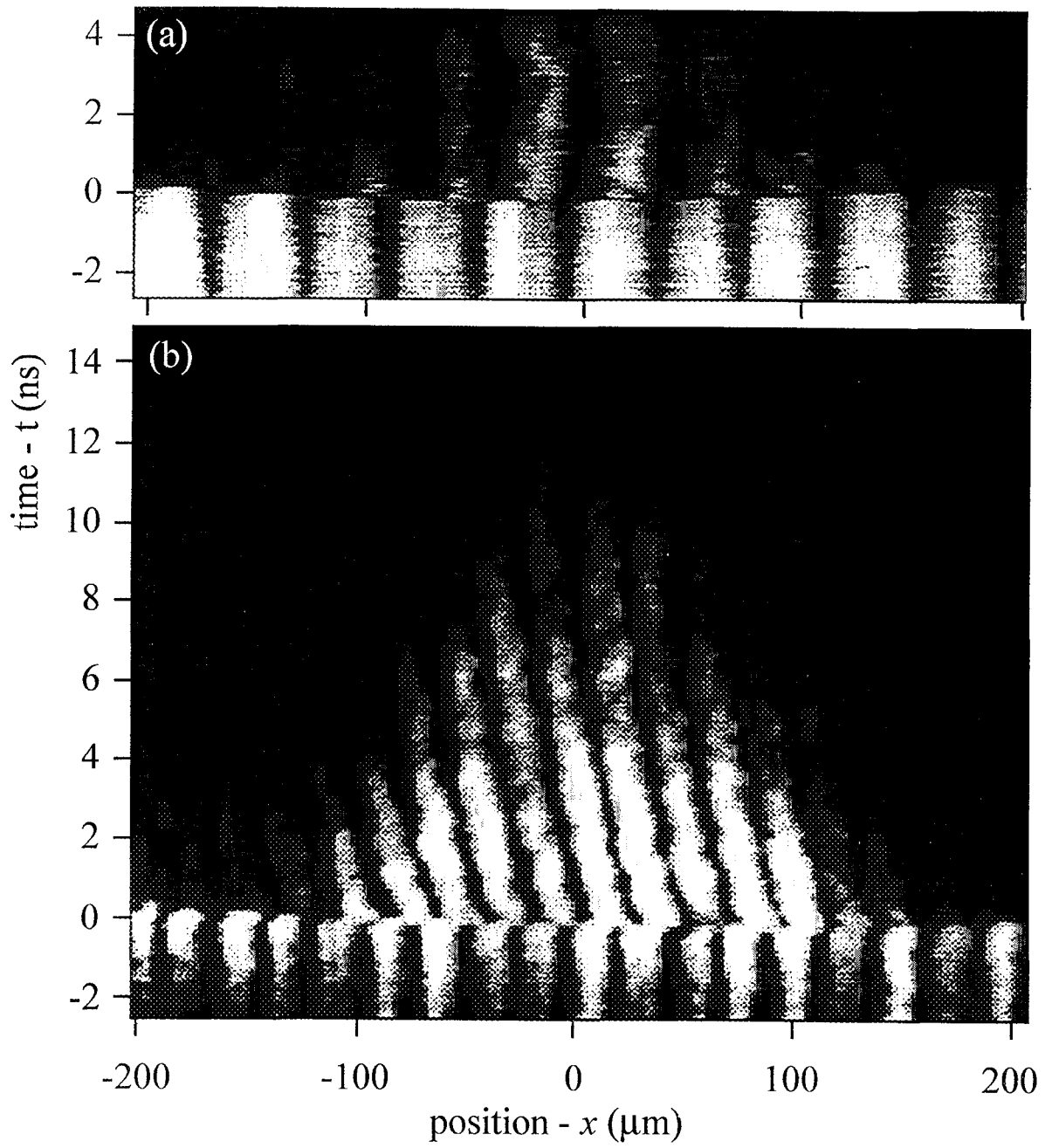


Figure 2.

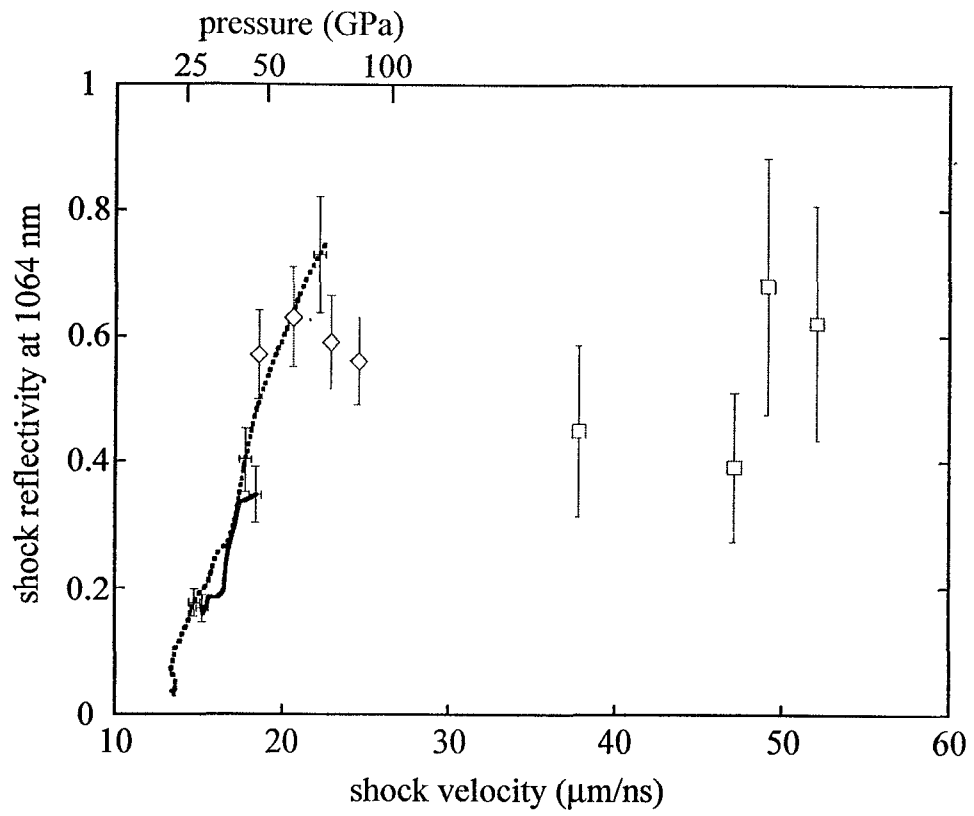


Figure 3.

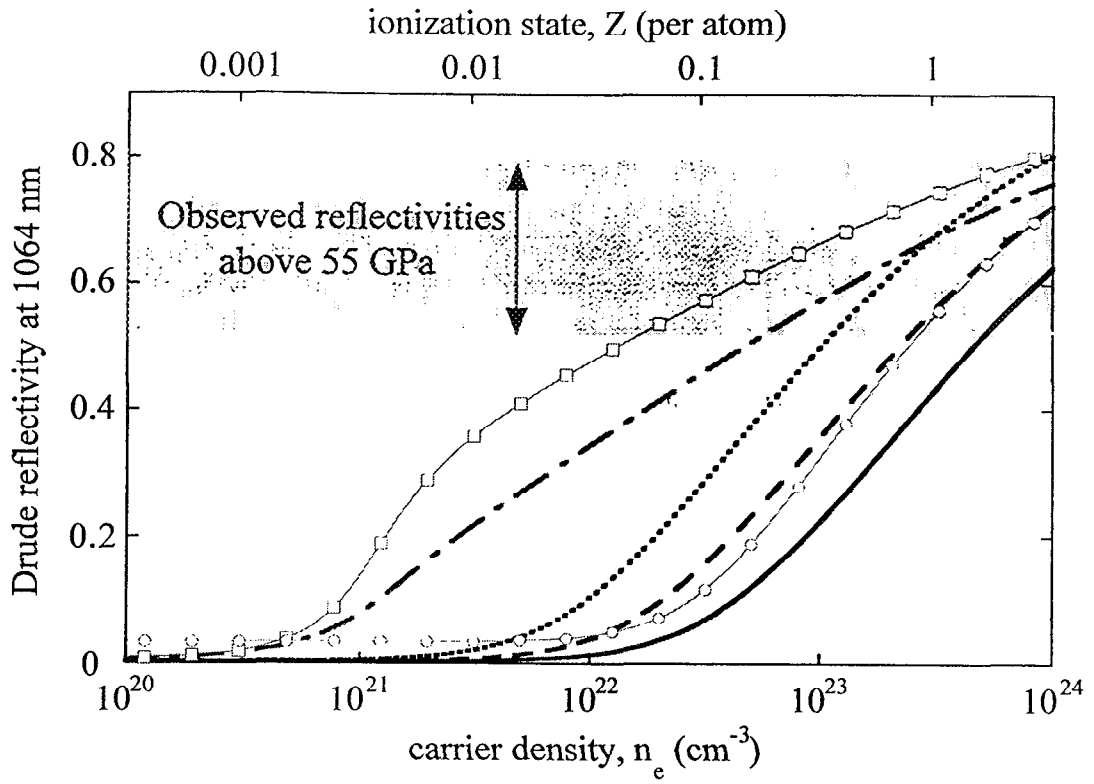


Figure 4.

